Energetics of the Electron Transfer from Bacteriopheophytin to Ubiquinone in the Photosynthetic Reaction Center of *Rhodopseudomonas Viridis*: Theoretical Study

Jun-ya Hasegawa,* Mayumi Ishida, and Hiroshi Nakatsuji*

Department of Synthetic Chemistry and Biological Chemistry, Graduate School of Engineering, Kyoto University, Yoshidahon-machi, Sakyo, Kyoto 606-8501, Japan

Zhenyu Lu, Haiyan Liu, and Weitao Yang

Department of Chemistry, Duke University, Durham, North Carolina 27708

Received: October 30, 2002

The energetics of electron transfer in the photosynthetic reaction center of *Rhodopseudomonas viridis* was studied using the density functional theory (DFT). By examining the basis set-dependence and the accuracy of the DFT for calculating adiabatic electron affinity, single-point calculations with 6-31+G(d) basis sets, at the geometry optimized with 6-31G(d) basis sets, were found to be almost independent of the basis set. In gas-phase calculations, bacteriopheophytin (H) had the greatest electron affinity among the three chromophores: H, menaquinone (MQ), and ubiquinone (UQ). However, the order of the electron affinity was reversed to be UQ > MQ > H by including residues that interacted with the chromophores through hydrogen bonding. Based on the QM/MM optimized geometries, cluster models for the binding sites were constructed. The computed reaction energy was comparable to values obtained experimentally. The reaction energy can be decomposed into a vertical electron affinity term and a relaxation energy term using a driving force analysis. The most important term was the vertical electron affinity of the chromophores. Based on optimization, there was little structural reorganization. The present results indicate that, with regard to the energetics of electron transfer, local interactions between the chromophores and proteins play a decisive role by tuning the electron affinity of the chromophores, whereas the effects of distant residues are of secondary importance.

1. Introduction

Photosynthesis by green plants and photosynthetic bacteria is one of the most important biochemical reactions on Earth. A key reaction in photosynthesis is photoinduced electron transfer in the photosynthetic reaction center protein (for reviews see refs 1−5).[1−5] Figure 1 shows the X-ray structures of the chromophores in the reaction center of *Rhodopseudomonas viridis* (*Rps.*).[6,7] An excited electron at the special pair (P) is transferred along the L-branch to bacteriochlorophyll *b* (B_L), bacteriopheophytin *b* (H_L), menaquinone (MQ), and finally ubiquinone (UQ). This electron transfer is known to be very effective, with a quantum yield of almost 100%. Therefore, a significant amount of effort has been concentrated on elucidating the mechanisms of various electron transfers in the reaction center. Although the chromophores are arranged in close to C_2 symmetry, the electron transfer from P to UQ occurs only along the L-branch. In addition to the important contributions from experimental studies on this point (for reviews, see refs 4 and 5), many theoretical studies have also provided useful insight. To understand the initial step in this electron transfer ($P \rightarrow H_L$), the absorption spectrum of the reaction center of *Rps.* was assigned.[8−13] The energetics of the initial steps in electron transfer was evaluated using electrostatic calculations,[14−16] the charge equilibration method,[17] molecular dynamics calculations,[18] and semiempirical quantum mechanical calculations.[9−11] The L-side selective transfer can mostly be ascribed to the electronic factor in the rate constant given by Marcus and Sutin,[19] based on semiempirical[10,14,15] and ab initio SAC−CI[20] studies.[21]

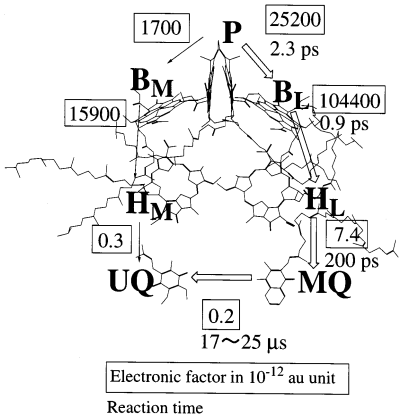

Figure 1. Chromophores in the photosynthetic reaction center of *Rhodopseudomonas viridis*. Numbers in the box denote the calculated electronic factor in 10^{-12} au unit.[21,39] Numbers under the box are the observed reaction time. The nuclear coordinates are taken from 1PRC[6] in Protein Date Bank.[7]

The slow electron transfer from H to MQ and from MQ to UQ shows complex characteristics. A recent review article by Okamura et al.,[22] mainly about *Rhodobacter sphaeroides* (*Rd.*), provides considerable insight. The first excited electron is transferred from H to Q_A (MQ in *Rps.* and UQ in *Rd.*) with a rate constant of $k_{H\rightarrow MQ} = 4.4 \times 10^9$ (s^{-1})[23] and then to Q_B (UQ in both *Rps.* and *Rd.*) with $k_{MQ\rightarrow UQ} = 10^4$ (s^{-1}).[22] Stowell et al.

* To whom correspondence should be addressed. E-mail: hasegawa@sbchem.kyoto-u.ac.jp; hiroshi@sbchem.kyoto-u.ac.jp. Fax: +81-75-753-5910.

10.1021/jp022334b CCC: $25.00
Published on Web 12/28/2002

TABLE 1: Adiabatic Electron Affinity of Quinones in the Gas Phase Computed by DFT with Various Basis Sets[a]

basis sets	E_n(a.u.)[b]	E_a(a.u.)[b]	adiabatic electron affinity (EA) in kcal/mol	adiabatic electron affinity (EA) in eV
		(1) p-Benzoquinone(p-BQ)		
6-31G	−381.341554	−381.410191	43.1	1.87
6-31G(d)	−381.451687	−381.509915	36.5	1.58
6-31+G	−381.359908	−381.448701	55.7	2.42
6-31+G(d)	−381.470458	−381.550012	49.9	2.16
6-31+G(d) SP[c]	−381.470431	−381.549899	49.9	2.16
6-311+G(2d,p)	−381.572506	−381.650840	49.2	2.13
CASPT2/ANO-L+diffuse[d]			46.4	2.01
SAC−CI/Huzinage−Dunning TZ2P + Diff, Ryd[e]			38.5	1.67
exptl.			44.0,[f] 42.9[g]	1.91,[f] 1.86[g]
		(2) 2,3,5,6-Methyl-1,4-p-benzoquinone(2,3,5,6-Me-1,4-pBQ)		
6-31G(d)	−538.733131	−538.782331	30.9	1.34
6-31+G(d)	−538.751770	−538.818026	41.6	1.80
6-31+G(d) SP[c]	−538.751691	−538.817860	41.6	1.80
exptl.			37.4[f]	1.62[f]
		(3) 1,4-Naphthoquinone(1,4-NQ)		
6-31G(d)	−535.115947	−535.170163	34.0	1.49
6-31+G(d)	−535.137357	−535.210516	45.9	1.99
6-31+G(d) SP[c]	−535.137318	−535.210412	45.9	1.99
6-311+G(2d,p)	−535.273331	−535.345715	45.4	1.97
exptl.			41.7[f]	1.81[f]
		(4) 2-Methyl-1,4-Naphthoquinone(2-Me-1,4-NQ)		
6-31G(d)	−574.438347	−574.489576	32.1	1.39
6-31+G(d)	−74.459990	−574.529586	43.7	1.89
6-31+G(d) SP[c]	−574.459937	−574.529466	43.6	1.89
exptl.			40.1[f]	1.74[f]

[a] Some previous results and experimental data are also shown. [b] E_n and E_a are abbreviations for total energy at the optimized geometry of neutral and anion species, respectively. [c] Single-point calculation at a geometry optimized by DFT/B3LYP with 6-31G(d) basis sets. [d] Reference 70. ANO-L C,O[4s3p1d],H[2s1p], diffuse 1s1p1d at the center of the molecule. [e] Reference 71. Huzinage−Dunning TZ + polarization and diffuse functions (C[6s4p2d], O[7s5p2d], and H[3s2p]) and Rydberg 2s2p2d functions at the center of the molecule. [f] Reference 42. [g] Reference 43.

successfully crystallized the "light" and "dark" structures of the reaction center of *Rd*.[24] Graigh et al. found that the rate constant is independent of the driving force (ΔG) by driving force assay.[25] These facts indicate that the rate-limiting step is the conformational gating step.[25] For *Rhodopseudomonas viridis*, the same mechanism can be expected because of the structural similarity between *Rps.* and *Rd*. Thus, after the reduction of MQ, UQ at the distal position moves into the proximal position (Q_B site) and then accepts an electron from MQ.

Many theoretical studies have been reported over the past 10 years. Studies using classical simulation methods have concentrated on the kinetics,[26] protein motion,[27,28] and the reorganization of the protonation state of ionizable residues in the reaction center.[29−33] It was found that relaxation of the protein structure is important for reproducing the experimental reaction free energy.[30,32] However, these studies were within the classical approximation even for chromophores for which the electronic states and charge distribution change in the course of electron transfer. Some semiempirical INDO MO studies[34,35] have been reported, but their computational models for protein residues might be inadequate for treating energetics. Recently, a DFT study[36] was reported for *Rhodobacter sphaeroides*, in which the protein effect was modeled by two water molecules for hydrogen-bonding and by the self-consistent isodensity polarizable continuum model (SCIPCM)[37,38] for the dielectric effect. They successfully reproduced the energetics, although the proximal protein residues may be oversimplified in their computational model. Furthermore, they showed that the electron affinity of the quinones depends significantly on solvation by the protein. A different approach is based on the electronic factor in the rate constant formula[19] using quantum mechanical calculations.[39] The computed electronic factor was unexpectedly so large it suggested that electron transfer might be regulated by some other rate-limiting step, like the conformational gating mechanism.[22]

One puzzling issue involves the electron affinities of quinones and bacteriopheophytin in the reaction center. Because bacteriopheophytin has a large π-electron system with a low LUMO energy level, its electron affinity is quite large (90 kcal/mol in DMF[40]). Quinones are also very strong electron acceptors, with a large electron affinity in water (around 100 kcal/mol[41]) and a smaller electron affinity in the gas phase (around 40 kcal/mol).[42,43] A comparison of theoretical calculations in the gas phase shows that bacteriopheophytin has a greater electron affinity (45kcal/mol) than quinones (35 kcal/mol), as shown in Table 2, indicating that electron transfer is difficult to explain without considering the effects of surrounding protein residues. Therefore, quantum chemical calculations for electron affinity should include the effects of surrounding proteins, which might be essential as a driving force for electron transfer. In a similar system, *Rhodobacter sphaeroides*, Blomberg et al.[36] showed that hydrogen bonding and the dielectric effect both significantly affect electron affinity.

Another interesting point is the reaction coordinate of the electron transfer. As shown in Figure 1, electron transfer from MQ to UQ is slow. In addition, the reduced UQ is a stable intermediate.[22] Thus, there should be enough time for structural relaxation of the system after electron transfer. However, there has not yet been a careful study on whether the reaction coordinate is within the chromophores or extends to the solvation structure in the protein. A recent development in the QM/MM methodology[44−46] makes it possible to calculate the minimum-energy structure before and after electron transfer in proteins.

The thermodynamic parameters estimated based on experimental results are $\Delta G = 0.65$ eV (15.0 kcal/mol) for $H \rightarrow MQ$[47] and $\Delta G = 0.131$ eV (3.02 kcal/mol), $\Delta H = 0.076$ eV (1.75

TABLE 2: Vertical Electron Affinity (vEA) (in kcal/mol) of the Chromophores calculated by DFT with the B3LYP functional

method	gas phase[a]	+residues[b,c]	+RF[b,d]	+SCRF[b,e]
(a) H(bacteriopheophytin)				
B3LYP/6-31+g(d)	47.3	54.5	52.1	64.3 (9.8)
(b) MQ(menaquinone)				
B3LYP/6-31+g(d)	38.0	69.0	68.5	76.4 (7.4)
(c) UQ(ubiquinone)				
B3LYP/6-31+g(d)	36.2	72.6	71.2	82.4 (9.8)

[a] Geometry was optimized for neutral state in the gas phase. [b] Geometry was optimized for neutral state by the QM/MM calculations. [c] Binding site model 2 shown in Figure 2. [d] Onsanger reaction field with the dipole approximation has been included in addition to the binding site models. The dielectric constant for acetone, 20.0, is used. [e] Self-consistent reaction field effect estimated with the 6-31g(d) basis sets has been included in addition to the binding site models. The values in parentheses indicate the change of vEA from the "+residues" calculations.

kcal/mol) for MQ → UQ.[48] However, the origin of the driving force is still ambiguous. These thermodynamic parameters can be decomposed into simple molecular properties: vertical electron affinity (vEA) and relaxation energy (ER) terms. Hereafter, we call this decomposition analysis the driving force analysis (DFA). The vEA and ER terms reflect, respectively, the electronic and structural relaxations of the system after reduction of the chromophores. A quantum chemical DFA study is quite useful for understanding the origin of the driving force of the electron transfer in terms of vEA and ER.

We have been studying electron transfer in the photosynthetic reaction center in *Rhodopseudomonas viridis*. In a series of studies on the absorption spectrum, SAC−CI calculations gave an ab initio assignment for the reaction center.[12,13,49] An SAC−CI study revealed that the L-branch preference of the electron transfer is mostly due to electronic factors.[12,21] A perturbation-theoretical method was applied to the electronic factor for electron transfer from H to UQ along both the L and M chains[39] and for electron transfer from the cytochrome *c* unit to the oxidized special pair P^+.[50]

The results reported here are part of our quantum-chemical study of electron transfer in the reaction center of *Rhodopseudomonas viridis*. In this paper, we describe the energetics of the electron transfer from H to MQ and from MQ to UQ. Quantum chemical calculations for the chromophores are performed using density functional theory (DFT). We sought (1) to investigate how proteins affect the electron affinities of MQ and UQ to pass an electron from H to UQ, (2) to find the energy-optimal structure after reduction to identify the reaction coordinate of the electron transfer, (3) to evaluate the energy level diagram against the electron-transfer coordinate, and (4) to clarify by DFA the characteristics of the electron transfer in terms of electronic and structural relaxations during electron transfer. Section 2 explains the computational details and section 3 describes the numerical results, i.e., vEA with and without protein effects, and the theoretical and experimental results are compared with regard to the energetics of electron transfer. In section 4, the energetics is analyzed in terms of structural effects and DFA.

2. Computational Details

2.1. Computational Models. Figure 2 shows computational models for the H-, MQ-, and UQ-binding sites. They are composed of chromophores and some proximate amino acid residues that interact with the chromophores through hydrogen bonds. For the chromophores, the phytyl groups in H and MQ are simplified to methyl groups. Because H is located in a hydrophobic part of the protein, only two residues are included. The structures shown are the subject of the present quantum chemical calculations, and the effect of the remaining protein is taken into account by a continuum model with a spherical cavity[51] or by the self-consistent reaction field (SCRF) method with the SCIPCM.[37,38] For the SCRF calculations, a dielectric constant of 4.0 as suggested by the previous study[36] was used. (See Appendix.) For MQ and UQ, two models, Models 1 and 2, are shown. Based on a structural analysis of the optimized geometry by the QM/MM method,[44−46] model 1 is augmented by a residue and some substituents to form model 2. In particular, Asn M257 is added to MQ in model 2, because the effect of this residue was found to be nonnegligible after the result of the present QM/MM calculations were analyzed. The charge polarization in the main chain mainly contributes to the stabilization of MQ in the anion state, because the main chain of Asn M257 is close to one of the oxygen atoms in MQ.

In the QM/MM method, the self-consistent charge density-functional based tight-binding (SCC-DFTB) method[52] is used to optimize the initial- and final-state geometries of the QM parts, menaquinone and ubiquinone, within the protein environment. The implementation of SCC-DFTB QM/MM is described in refs 53 and 54. The MM energy and force are calculated by the TINKER program,[55] and AMBER-95 is used for the force field.[56]

The protonation states of titratable residues are assigned using the following guidelines: (1) Residues close to the protein surface are considered neutral because they must be neutralized by counterions. (2) Residues with counterionic residues are left ionized. For example, in a pair consisting of GLU and ARG, both residues are ionized. In this way, the pair considered together is neutral. (3) In rare cases, residues in a hydrophobic environment remain neutral, because there is no apparent proton acceptor in the region. For residues close to the protein surface, a more elaborate model would include the solution and the counterions surrounding the protein. Fortunately, the structure obtained for neutral chromophores agrees reasonably well with the experimental structure (2PRC),[57] as shown later in Figure 6. We expect that the charges on the protein surface are more or less compensated at the chromophore binding site and provide only a minor contribution to the electrostatic potential at the binding site.

For the initial state, the total charges on menaquinone and ubiquinone are −1 and 0, respectively. For other cofactors, the total charge on P is assumed to be +1 and 0 for B and H; +2 is assumed for metal ions. We follow a recently developed iterative optimization method.[46] The partial charges for the cofactors are calculated by SCCTB, and the protein structure is then optimized until the RMSD energy gradient is below 1.0 kcal/mol/Å. The geometries of the cofactors P, B, H, and ions are kept fixed during the optimization. Next, the geometries of menaquinone and ubiquinone are optimized within the relaxed protein environment using the QM/MM method. The same procedure is used for the final state except that the total charges for menaquinone and ubiquinone are switched.

2.2. Method and Basis Sets. The electron affinities of the chromophores were calculated by DFT[58−61] using the B3LYP functional.[62,63] The 6-31G(d) basis sets (6-31G sets[64] plus a single polarization d-function[65] on carbon, nitrogen, and oxygen) were used for geometry optimization, and the 6-31+G(d) sets (6-31G(d) sets plus 1s1p diffuse functions on carbon, nitrogen, and oxygen[66]) were used for single-point calculations at the

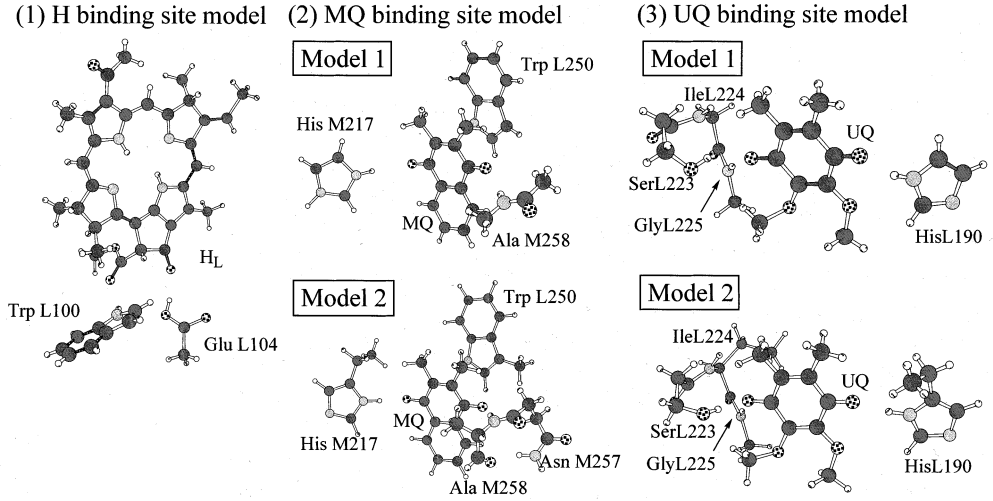

Figure 2. Binding site models for (1) H, (2) MQ, and (3) UQ, respectively.

optimized geometry. For the hydrogens in hydrogen bonds between the amino acid residues and quinones, an additional p-type polarization function[65] was augmented.

DFT is a practically useful electronic structure theory, especially if the computing target is very large, as in biological systems. Although its computational cost is almost the same as that of the Hartree−Fock method, DFT includes electron correlations that are often important for describing the potential energy of chemical reactions. However, because of the semiempirical nature of the functional, one should examine beforehand the numerical performance of DFT on the systems being studied. Before choosing the method and the basis sets described above, we performed several test calculations on adiabatic electron affinity for some benzoquinones and naphthoquinones: p-benzoquinone (pBQ), 2,3,5,6-methyl-1,4-p-benzoquinone (2,3,5,6-Me-1,4-pBQ), 1,4-naphthoquinone (1,4-NQ), and 2-methyl-1,4-naphthoquinone (2-Me-1,4-NQ). Benzoquinones and naphthoquinones have skeleton structures similar to ubiquinone and menaquinone, respectively. To accurately compute the adiabatic electron affinity, both the electronic and structural relaxation effects must be included correctly.

First, to check the basis set-dependence in computing the electron affinity, we performed DFT calculations of p-BQ starting with the 6-31G sets. As seen in Table 1 (1), adding a polarization d-function and diffuse s- and p-functions (namely 6-31+G(d) sets) causes a significant change in the electron affinity. However, further improvements (valence triple-ζ,[67] second polarization d-function[68] on C, N, and O, and polarization p-function on H) produced only a slight change of less than 1 kcal/mol. Similar results were seen for 1,4-NQ. Therefore, 6-31+G(d) sets are considered to be sufficient for the present calculations of electron affinity.[69]

Next, basis set convergence on the structure was examined. At the geometry optimized with 6-31G(d) sets, single-point calculations were performed with 6-31+G(d) sets. As seen in Table 1, the results of the single-point calculations are very close to those for the optimization with 6-31+G(d) sets with regard to the total energy and electron affinity for the test compounds. The geometry is almost converged with 6-31G(d) sets. Therefore, we concluded that the 6-31+G(d) single-point calculation at 6-31G(d) geometry could give results that were almost independent of the basis set.

In closing this section, we compare the computed adiabatic electron affinity with the experimental value[42,43] and with the results of previous calculations.[70,71] The DFT with 6-31+G(d) sets overestimates the electron affinity for all four quinones by 4∼6 kcal/mol. This constant overestimation does not complicate our discussion, because the error can be estimated and the constant shift can be canceled out when the difference in electron affinity is evaluated. The reaction energy, ΔE, which will be discussed later, is not affected by this overestimation, because it depends on the difference in adiabatic electron affinity, as described later. For p-BQ, previous results are available for comparison. The CASPT2[70] and SAC-CI[71] results show good agreement with the experimental values. Although the present DFT results do not agree as very closely with the experimental values, the computing time is much less. Because our target in this study is a very large system, we adopted DFT in the present calculations using the Gaussian 98[72] and 94[73] packages.

3. Results

3.1. Vertical Electron Affinity. In Table 2, the vertical electron affinity (vEA) computed for the chromophore is shown. Geometries optimized for the neutral states were used.

In the gas phase, H (bacteriopheophytin) has the largest vEA of the three chromophores: the vEAs of H, MQ (menaquinone), and UQ (ubiquinone) are 47.8, 34.5, and 31.7 kcal/mol, respectively. This means that the energies of the anionized states of MQ and UQ are higher than that of H, which is quite puzzling because an electron is transferred from H to UQ in the reaction center. Because there are no experimental data available on gas-phase vEA for the chromophores, we could not assess the accuracy of the computed values. However, the difference in vEA values is more than 10 kcal/mol, which is greater than the error in the calculations.

Next, we examined the effect of protein residues in the vicinity of the chromophore, since the electron affinities of quinones are known to be solvent-sensitive. We calculated the vEAs of chromophores within the binding sites: here, vEA is the difference in total energy between the anionized and neutral states in cluster models of the binding sites. Figure 2 shows computational models of the binding sites. As shown in Table 2, solvation by the residues increases the vEAs of the quinones by more than 20 kcal/mol. As a result, the relative magnitude of vEA changes to UQ > MQ> H, consistent with the observed electron transfer in the reaction center.

The significant solvation effect for quinones can be understood based on an analysis of their singly occupied molecular orbitals (SOMOs). Because the SOMOs of anion species have

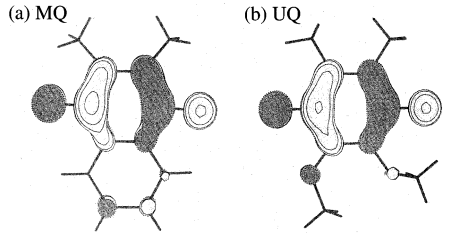

Figure 3. Singly occupied molecular orbital (SOMO) of (a) MQ and (b) UQ.

a large amplitude on the oxygen atoms of carbonyl groups (Figure 3), the quinone anion is greatly stabilized by solvation. UQ has the greatest effect, because several interacting residues exist in the binding site of UQ. The effect of the remaining protein was examined with a continuum model in a spherical cavity (Onsanger model)[51] and with the SCRF model. In the first model, the dielectric effect was small, as shown in Table 2. In a previous study,[36] however, the dielectric field greatly affected the electron affinity. Although the present protein models include actual residues surrounding the quinones, this discrepancy could be because of the method used to treat the dielectric field, because the Onsanger model used in this study could underestimate the dielectric effect. Therefore, the SCRF-(SCIPCM) effect was included in the calculations. The SCRF method stabilized the anion states and the vEA of the chromopores increased about 7.4∼9.8 kcal/mol. However, these changes in vEA are almost equal in the three chromophores.

The present results indicate that *the local protein environment plays a very important role in the energetics of electron transfer in the reaction center*. These calculations, however, do not include the structural relaxation effect. In the next subsection, we investigate the energetics of electron-transfer including this effect.

3.2. Energetics of Electron Transfer from Bacteriopheophytin (H) to Ubiquinone (UQ). To understand the energetics of this electron transfer, calculation of the vEA computed at the X-ray geometry alone is, of course, insufficient, because the reaction time for each step in electron transfer from H to UQ seems to be long enough for relaxation of the molecular structure to occur. In this subsection, we calculate the energies of the chromophores for the neutral and anion optimized structures and estimate the reaction energy for electron transfer and compare the results with the experimental data. An analysis of the results in terms of electron affinity, relaxation energy, and optimized structure will be presented later.

Electron-transfer involves two steps and three states: H^-, MQ^-, and UQ^-. H^- consists of H in an anion state and MQ and UQ in neutral states. MQ^- and UQ^- are defined similarly: MQ and UQ in an anion state and the remaining chromophores in a neutral state. Three sets of geometries are also defined: in the "initial-state geometry", the geometry of H was optimized for the anion state and those of MQ and UQ were optimized for the neutral state. The "intermediate-" and "final-state geometries" have anion structures for MQ and UQ and neutral structures for the other chromophores, respectively. The energies of the states are defined by summing the energies of the three chromophores:

$$\begin{cases} H^-\text{state: } E^{H^-\text{state}}(X) = E^{H^-}(X) + E^{MQ}(X) + E^{UQ}(X) \\ MQ^-\text{state: } E^{MQ^-\text{state}}(X) = E^{H}(X) + E^{MQ^-}(X) + E^{UQ}(X) \\ UQ^-\text{state: } E^{UQ^-\text{state}}(X) = E^{H}(X) + E^{MQ}(X) + E^{UQ^-}(X) \end{cases} \quad (1)$$

X denotes the geometry defined above, i.e., the initial-, intermediate-, or final-state geometry. This is a good approximation, because previous calculations showed that the electronic interaction between the chromophores is very small.[39]

Table 3 shows the relative energies of the states involved in the electron transfer. The H^- state at the initial-state geometry is taken as a reference. For the UQ^- state at the final-state geometry, the relative energy from the MQ^- state at the intermediate-state geometry is also shown in parentheses for comparison with experimental findings.[48] Actual electron transfer is expected to start with the H^- state at the initial-state geometry, pass through the MQ^- state in the intermediate-state geometry, and end up with the UQ^- state in the final-state geometry.

Energetics Computed from the Model Optimized in the Gas Phase. First, the energetics of electron transfer was studied using the geometry of the chromophores optimized in the gas phase. As shown in Table 3 ((1) C), the gas-phase model that includes only the isolated chromophores obviously cannot explain the energetics of electron transfer. The energy of the MQ^- state at the intermediate-state geometry is 3.8 kcal/mol higher than that of the H^- state at the initial-state geometry, which is completely different from the experimental free energy of −14.9 kcal/mol.[47] Therefore, because proteins significantly affect the electron affinity, as elucidated in the previous section, the interacting residues shown in model 1 in Figure 2 were attached to the chromophores, as in the X-ray structure.[6] Here, the energy of a state is defined as the sum of the energies of the binding-site cluster models, as in eq 1. The relative energy of the MQ^- state at the intermediate-state geometry is reduced to −3.4 kcal/mol: the potential surface of electron transfer from H to MQ slopes downward ((1) C+Res in Table 3). However, for the relative energy from the UQ^- state to the MQ^- state, this cluster model gave a worse agreement with the experimental findings.[48] This may be ascribed to the cluster model, which does not include Asn M257 in the MQ site. This residue affects the reaction energy, as described below. The remaining protein effects were included by further adding the reaction field with a spherical cavity model.[51] The relative energy was slightly modified by a few kcal/mol. However, we note that the present calculations could underestimate the dielectric effect,[36] because of the Onsanger model.

Energetics Computed from Models Optimized in the Binding Sites. The second computational model was constructed by optimizing the structures and positions of the chromophores in the binding-site cluster model. During optimization, the geometry of the protein residues was fixed according to the X-ray structure, except for the positions of the hydrogens involved in hydrogen-bonding with the chromophores. Because chromophore−residue interaction was already included in the model, the computed energy qualitatively reproduced the experiments ((2) C+Res in Table 3). The relative energy of the MQ^- state at the intermediate-state geometry is improved slightly to −6.0 kcal/mol. However, the energy of the UQ^- state is still underestimated, which again could be attributed to a lack of Asn M257 in the model.

Energetics Computed from Models Based on QM/MM Structures. The final model is also a binding-site cluster model, but the geometries adopted for the intermediate (MQ^-) and final (UQ^-) states were optimized by the QM/MM method.[44−46] For the geometry of H, the former structure optimized within the binding-site cluster model was used. In QM/MM calculations, the QM part included MQ and UQ and the rest of the protein was treated by the MM method. Optimization was performed

TABLE 3: Relative Energy Levels (kcal/mol) for (H$^-$)−MQ−UQ, H−(MQ$^-$)−UQ, and H−MQ−(UQ$^-$) States at Initial-, Intermediate-, and Final-State Geometries[r]

	initial-state geometry[a]			intermediate-state geometry[b]			final-state geometry[c]			
model	H$^-$	MQ$^-$	UQ$^-$	H$^-$	MQ$^-$	UQ$^-$	H$^-$	MQ$^-$	UQ$^-$	
(1) Optimized Geometry in the Gas Phase										
C[d]	0.0	14.7	16.4	4.5	3.8	15.6	8.3	17.6	0.0	(−3.8)[g]
C+Res[e]	0.0	0.3	12.1	11.2	−3.4	−6.3	20.7	15.5	−14.6	(−11.2)
C+Res+RF[f]	0.0	−0.3	14.8	11.1	−4.0	−3.6	18.4	12.6	−13.4	(−9.4)
C+Res+RF+ES(P$^+$)[h]	0.0				−1.9					(−9.5)
(2) Optimized Geometry in the Binding Site Model										
C+Res	0.0	3.6	4.1	12.2	−6.0	−0.4	17.6	13.4	−18.4	(−12.4)
C+Res+RF	0.0	−0.3	5.7	12.3	−9.4	2.2	17.2	10.0	−16.4	(−7.0)
C+Res+RF+ES(P$^+$)	0.0				−7.3					(−6.9)
(3) QM/MM Optimized Geometry for MQ and UQ (Asn M257 in MQ Site Is Included in the Model)										
C+Res	0.0	−6.8	−10.4	13.6	−12.2	−4.5	21.6	7.1	−14.0	(−1.8)
C+Res+RF	0.0	−9.6	−12.3	13.6	−14.2	−5.5	21.2	4.8	−15.6	(−1.4)
C+Res+SCRF[q]	0.0	−4.9	−10.9	13.9	−9.0	−4.2	21.2	9.1	−14.0	(−5.0)
C+Res+RF+ES(P$^+$)	0.0				−12.1				−13.6	(−1.5)
C+Res+SCRF+ES(P$^+$)	0.0				−6.9					(−5.1)
exptl.	0.0				−15.0[i]					(−1.75[j])
previous theoretical[k]	0.0				−14.9[l], −11[m]					(−3.4[n], −3.6[o], −1.8[p])

[a] H: anion structure. MQ and UQ: neutral structure. [b] MQ: anion structure. H and UQ: neutral structure. [c] UQ: anion structure. H and MQ: neutral structure. [d] Chromophores. [e] Protein residues are included in the model. [f] Onsanger reaction field is included in the model. Dielectric constant is 20.0 (acetone). [g] The values in parentheses are the relative energy from the MQ$^-$ state at the intermediate−state geometry. [h] Electrostatic interaction between the special pair in the cation state and the chromophore is included. See text. [i] Reference 47. [j] Reference 48. [k] Previous theoretical studies. [l] DFT calculation for *Rhodobacter sphaeroides*, reference 36. [m] Reference 26. [n] Free energy calculation, reference 27. [o] Free energy calculation, reference 29. [p] Free energy calculation for *Rhodobacter sphaeroides*, reference 32. [q] Self−consistent reaction field effect estimated with the 6-31g(d) basis sets is included. See the appendix. [r] H$^-$, MQ$^-$, and UQ$^-$ indicate the (H$^-$)−MQ−UQ, H−(MQ$^-$)−UQ, and H−MQ−(UQ$^-$) states, respectively. The energy of the H$^-$ state in the initial-state geometry is taken as a reference.

for the entire protein structure in the intermediate and final states. For the QM calculations, an approximate DFT, the self-consistent charge tight binding (SCCTB) method,[52] was adopted. In constructing the cluster models based on the QM/MM results, the models were extended to some extent to include chromophore-residue interactions in the QM/MM optimized structures, as shown in model 2 in Figure 2. For the model of the MQ binding site, Asn M257 in the proximity of MQ turned out to contribute to the reaction energy, and therefore this residue was also included in the cluster model. The proximate interacting residues included in this model are those that contribute more than 3 kcal/mol to the reaction energy.

Using these extended models, the computed ΔE(H → MQ) was improved to −12.2 kcal/mol, which is close to the experimental value of −15.0 kcal/mol (Table 3 (3) C+Res). ΔE(MQ→UQ) was also significantly improved to −1.8 kcal/mol, which is also comparable to the experimental value of −1.75 kcal/mol. This improvement in the relative energy might be mostly due to refinement of the cluster model and especially to the addition of Asn M257, which will be discussed later. The dielectric effect of protein treated by the Onsanger model gave small corrections, whereas that by the SCRF method worsened the agreement with the experimental values. Finally, a minor contribution of electrostatic interaction between a cationic special pair and other chromophores was included (C+Res+RF+ES(P$^+$) in Table 3). A dielectric constant of 4.0 is used, as in the previous study.[36] Table 3 shows that the interaction stabilizes the H$^-$ state more than the MQ$^-$ state by 2.1 kcal/mol. On the other hand, the UQ$^-$ state is stabilized more than the MQ$^-$ state by only 0.1 kcal/mol.

Using the proper geometry and proper binding-site cluster model, the computed reaction energy was improved toward the experimental findings. However, we could not rule out the possibility that the numerical results might be further influenced by the nonuniform MM electrostatic field from residues that are not included in the current cluster models.

4. Discussion

4.1. Driving Force Analysis: A Decomposition Analysis of the Reaction Energy. Because the computed reaction energies agree reasonably well with the experimental values, an analysis of the reaction energy could provide meaningful information. The computed reaction energy ΔE can be divided into two terms: vertical electron affinity (vEA) and relaxation energy (ER):

$$\Delta E = (\upsilon\mathrm{EA}^{\mathrm{donor}} - \upsilon\mathrm{EA}^{\mathrm{acceptor}}) + (\mathrm{ER}^{\mathrm{donor}} - \mathrm{ER}^{\mathrm{acceptor}}) \quad (2)$$

υEA and ER for a chromophore X are defined as follows: υEA is the energy difference between the anion and neutral species at the equilibrium structure of the neutral species and ER is the stabilization energy of an anion species when it is relaxed to the anion structure:

$$\mathrm{ER}^X = E^{X^-}(\text{neutral}) - E^{X^-}(\text{anion}) \quad (3)$$

$$\upsilon\mathrm{EA}^X = E^X(\text{neutral}) - E^{X^-}(\text{neutral}) \quad (4)$$

We note that ΔE can also be defined as the difference between the adiabatic electron affinities of the donor and acceptor:

$$\Delta E = \mathrm{EA}^{\mathrm{donor}} - \mathrm{EA}^{\mathrm{acceptor}} \quad (5)$$

Table 4 shows the results of the decomposition analysis for the two steps in the electron transfer, H → MQ and MQ → UQ.

4.2. Structural Analysis and Driving Force Analysis Binding-Site Model using the Gas-Phase Optimized Geometry. As described in the previous section, the gas-phase calculations failed to reproduce the reaction energy for the step H → MQ. The decomposition in Table 4 ((1) C) shows that the reason for the positive reaction energy lies in the *υEA* term. Because the model does not include the proximate residues, *υEA* of H is larger than that of MQ by 9.3 kcal/mol. Although the relaxation energy of MQ is larger than that of H, ΔE becomes

TABLE 4: Decomposition Analysis for the Reaction Energy of the Electron Transfer in the Photosynthetic Reaction Center of *Rhodopseudomonas Viridis* (kcal/mol)

	H → MQ							MQ → UQ						
	υEA[a]			ER[a]				υEA			ER			
model	υEA^{H}	υEA^{MQ}	$\Delta\upsilon$EA	ER^{H-}	ER^{MQ-}	ΔER	ΔE	υEA^{MQ}	υEA^{UQ}	$\Delta\upsilon$EA	ER^{MQ-}	ER^{UQ-}	ΔER	ΔE
(1) Optimized Geometry in the Gas Phase														
C[b]	47.3	38.0	9.3	2.9	8.5	−5.6	3.7	38.0	36.2	1.8	8.5	14.0	−5.5	−3.7
C+Res[c]	51.7	56.9	−5.2	10.3	8.6	1.7	−3.5	56.9	69.3	−12.4	8.6	7.4	1.2	−11.2
C+Res+RF[d]	51.5	57.3	−5.8	10.3	8.6	1.7	−4.0	57.3	66.3	−9.0	8.6	9.0	−0.4	−9.4
(2) Optimized Geometry in the Binding Site Model														
C+Res	54.5	58.7	−4.2	5.2	7.1	−1.9	−6.0	58.7	66.3	−7.6	7.1	11.8	−4.7	−12.3
C+Res+RF	52.1	59.3	−7.2	5.3	7.3	−2.1	−9.4	59.2	62.0	−2.8	7.3	11.4	−4.1	−7.0
(3)QM/MM Optimized Geometry for MQ and UQ (Asn M257 in the MQ Site Is Included in the Model)														
C+Res	54.5	69.0	−14.5	5.2	2.9	2.3	−12.2	69.0	72.6	−3.6	2.9	1.1	1.8	−1.8
C+Res+RF	52.1	68.5	−16.5	5.3	2.9	2.4	−14.2	68.5	71.2	−2.7	2.9	1.7	1.2	−1.4
C+Res+SCRF[g]	64.3	76.4	−12.1	5.6	2.5	3.1	−9.0	76.4	82.4	−6.0	2.5	1.5	1.0	−5.0
Exptl.							−15.0[e]							−1.75[f]

[a] υEA and ER are abbreviations for the vertical electron affinity and relaxation energy, respectively. [b] Chromophores. [c] Protein residues are included in the model. [d] Onsanger reaction field is included in the model. Dielectric constant is 20.0 (acetone). [e] Reference 47. [f] Reference 48. [g] Self-consistent reaction field effect estimated with the 6-31g(d) basis sets is included. See appendix.

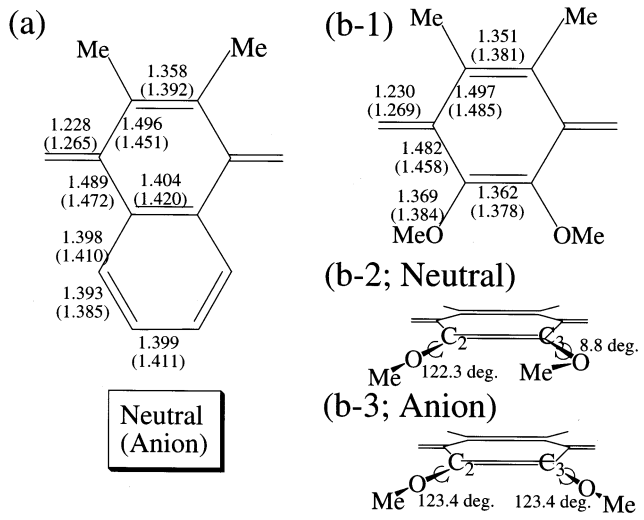

Figure 4. Structures of (a) MQ and (b) UQ optimized in the gas phase by DFT/B3LYP with 6-31g(d) basis set. In (b-1) and (b-2), dihedral angles, C_3-C_2-O-Me and C_2-C_3-O-Me, are shown. In (a) and (b), bond lengths of the neutral and anion (in the parenthesis) structures are shown in ångstrom unit.

3.7 kcal/mol. For the second step, MQ→UQ, the relaxation energy is −3.7 kcal/mol. Although $\Delta\upsilon EA$ is positive, the relaxation energy of UQ is larger than that of MQ by 5.5 kcal/mol. This large relaxation energy of UQ is related to rotation of the methoxy group. In Figure 4, the optimized structures of MQ and UQ are shown. Comparing (b-2) with (b-3), the dihedral angles differ by about 115°. In the neutral species, one of the two methoxy groups points toward the other methoxy group, which indicates the formation of intramolecular hydrogen bonds with the lone-pair in the other methoxy group. The methoxy group at the C_2 position appears to show hydrogen-bonding with the lone-pair in the carbonyl group. In the anion species, both of the methoxy groups prefer hydrogen-bonding to the carbonyl group, because the carbonyl oxygens in the anion species have larger minus charges, reflecting the character of the SOMO.

Table 4 also shows why attachment of the proximate resides improves the reaction energy of H → MQ and makes it negative ((1) C+Res). The electron affinity of MQ increases by about 19 kcal/mol because of the effect of the proximate residues. The electron affinity of UQ also shows a large increase of about 33 kcal/mol, which causes a large negative reaction energy of −11.2 kcal/mol.

The structural change in the skeletons is very small in all of the quinones. The bond-stretching tendencies reflect the characteristics of the SOMO. The C═O bonds are elongated by 0.04 Å, but the next C−C bonds are shortened. In comparison with Figure 3, the SOMOs have an antibonding character on the C═O bonds and a bonding character on the C−C bonds. Almost the same degree of skeleton relaxation can be seen in the binding-site models and in the QM/MM models. For bacteriopheophytin (H), the amount of this relaxation is quite small, and therefore we do not discuss it further.

Binding-Site Model using the Geometry Optimized in the Binding Site. Table 4 (2) shows the DFA for the second models: the geometry of the chromophores and hydrogens involved in hydrogen-bonding was optimized in the binding-site cluster model shown in Figure 2 (model 1). The geometry of the rest of the protein residue was fixed to the X-ray structure.[6] Because the proximate residues are included in the models, the ΔE's for both H → MQ and MQ → UQ are negative and similar to the (1)C+Res results. In the optimized geometry shown in Figure 5, the anionized chromophores are closer to the hydrogen-bonding residues. For the MQ site, the distance from the hydrogen in Ala M258 to the oxygen in MQ decreases by about 0.14 Å. The distance from the hydrogen in His M217 to the oxygen in MQ also decreases by about 0.25 Å. For the UQ site, similar behavior is observed. The O (UQ)−H (Ser L223) and O (UQ)−H (His L190) distances decrease by 0.13 and 0.25 Å, respectively. This is because anionized species experience a greater positive electrostatic field by moving closer to the residues. However, there is a large discrepancy between the X-ray (black lines) and optimized structures (blue lines), especially for the UQ site. This can be attributed to the oversimplified model used in the optimization. As for the skeleton of the chromophores, the amount of the displacement is similar to that in the gas-phase optimization and is very small.

The rearrangement in the hydrogen-bonding structure is also of interest, because a proton is transferred from Ser L223 in the step after the reduction of UQ.[22] Our calculations show that the positions of the hydrogen atoms involved in hydrogen bonding do not change much between the neutral and anion structures. These changes are within 0.01 Å. This result indicates that the proton transfer from Ser L223 requires a great deal of external perturbation, which helps Ser L223 to release the

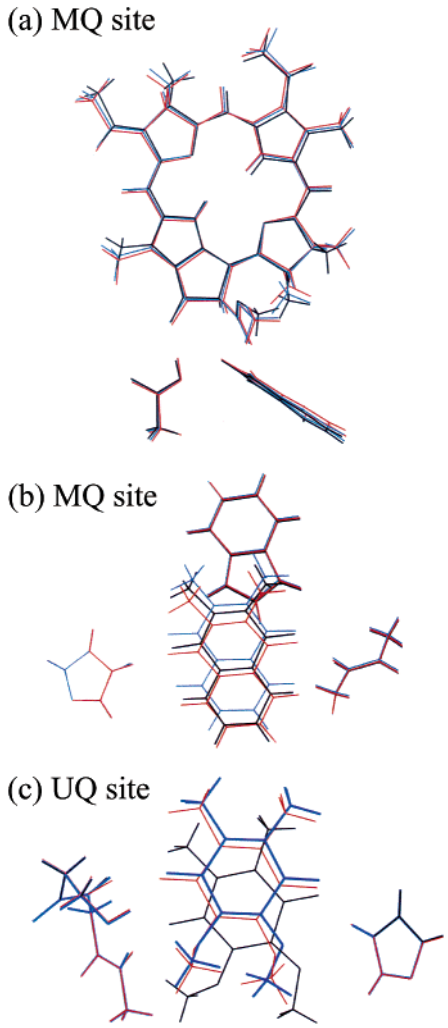

Figure 5. Molecular structure of (a) H, (b) MQ, and (c) UQ sites models. Geometries of the chromophores and the hydrogens in the H bonding are optimized. The rest of the protein residues is fixed to the X-ray geometry. The red, blue, and black lines represent the anion, neutral, and X-ray(2PRC)[57] structures, respectively.

proton. Thus, proton donation to Ser L223 from other acidic residues is likely necessary to trigger the protonation of UQ by Ser L223, as has been suggested in other reports.[22,74−76]

Binding-Site Models using the QM/MM Geometry. An analysis of this model clearly shows that the most important term is vEA of the chromophores. The ΔvEA term is larger than the ΔER term in both of the steps in electron transfer. Therefore, we conclude that *the vertical electron affinity, which is controlled by the residues, plays the definitive role in the energetics of electron transfer*. The ΔvEA term of −16.5 kcal/mol leads to a ΔE of −14.2 kcal/mol in H → MQ. For MQ → UQ; although the magnitude of ΔvEA is small, this is still the dominant term.

As explained in the last section, the third model taken from the QM/MM structure improves the values of ΔE for H → MQ and MQ → UQ, as seen in Table 4 (3). These results are comparable to the experimental data. We analyzed this result by DFA. First, for the vEA term, a comparison with the second model shows that the ΔvEA term is reduced by 10 kcal/mol in the H → MQ step and increased by 4.0 kcal/mol in the MQ → UQ step. The vertical electron affinity of MQ increases by 10 kcal/mol. This can mainly be attributed to the inclusion of Asn M257 in the computational model, because Asn M257 stabilizes the anionized state of MQ, which was also expected from the analysis of the preliminary QM/MM results. The change in EA caused by the inclusion of Asn M257 indicates that proper modeling of the local environment is very important. The local environment plays a crucial role in the energetics of the electron transfer.

There is also a decrease in the relaxation energy in the QM/MM model. The difference from the second model is about 4.2 and 6.5 kcal/mol in the H → MQ and MQ → UQ steps, respectively. Comparing Figure 6 with Figure 5, the structural rearrangement seen in the QM/MM geometry is much smaller than that in the second model. Especially in UQ, the large upper shift of about 1.5 Å seen in the second model (Figure 5) is not reproduced in the third model (Figure 6). In the anionized MQ site, the O(MQ)−H(Ala M258) and O(MQ)−H(His M217) distances are decreased by only about 0.05 and 0.07 Å, respectively, compared with the neutral MQ site. In the reduced UQ site, the O(UQ)−H(Ser L223) and O(UQ)−H(His L190) distances are decreased by about 0.09 and 0.19 Å, respectively, which is much less than with the second model. The positional shifts of the chromophores might be suppressed by other protein structures not included in the second model (model 1 in Figure 2). In the X-ray structure, Leu L189 is proximate to the methyl group of UQ. The edge-to-edge distance is about 2.5 Å, which is close enough so that UQ does not change its position as freely as in the second model. The rotation of the methoxy group in UQ can also be ascribed to the small relaxation energy. In the gas-phase model, the relaxation energy of UQ is 14.0 kcal/mol because of rotation, as seen in Figure 4. In the QM/MM optimizations, the neighboring residues hinder methoxy rotation and suppress the relaxation of UQ.

Conclusions

The energetics of the electron transfer in the reaction center of *Rhodopseudomonas viridis* was studied by DFT. The basis set-dependence and reliability of the DFT (B3LYP functional) for the present subject were examined by calculations of the adiabatic electron affinities of a series of quinones: p-benzoquinone (pBQ), 2,3,5,6-methyl-1,4-p- benzoquinone, 1,4-naphthoquinone, and 2-methyl-1,4-naphthoquinone. The single-point calculation with 6-31+G(d) basis sets at the geometry optimized with 6-31G(d) basis sets seems acceptable. The DFT tends to overestimate the electron affinity by 4∼6 kcal/mol. Fortunately, however, the present argument is based on the difference in electron affinity, so that this constant error is expected to be canceled out.

The electron affinities of quinones are shown to significantly depend on solvation by protein residues. *Especially, the local protein environment is very important, and the dielectric effect would be of secondary importance, as shown in Table 2.* The protein serves not only to fix the chromophores in space but also adjusts the energy levels by tuning the electron affinities of the quinones. Although bacteriopheophytin (H) has the greatest electron affinity among the three chromophores in the gas phase, the inclusion of hydrogen-bonding residues enhances the electron affinity of the quinones and reverses the order to UQ > MQ > H.

To study the energetics, three kinds of computational models, binding-site cluster models, were constructed. The proximate residues that interacted directly with the chromophores through hydrogen-bonding were included in the DFT calculations, and the rest of the protein effect was treated by the Onsanger and the SCRF(SCIPCM) models. Summing over the energies of the cluster models, the energy of the states involved in the electron transfer was evaluated. The model using the QM/MM geometry

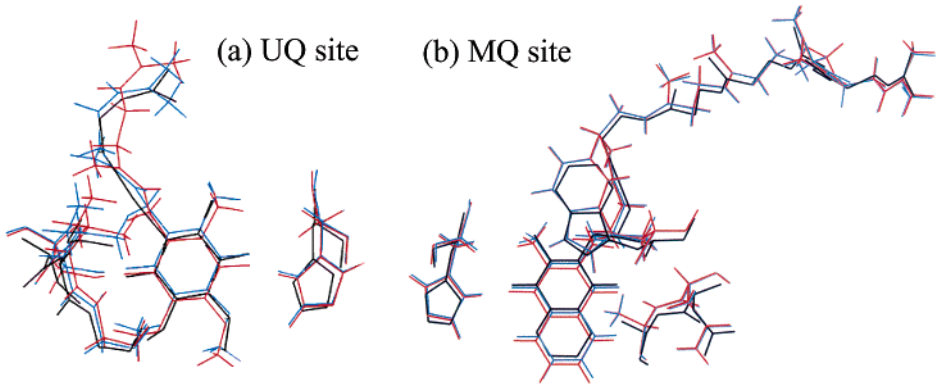

Figure 6. Molecular structure of (a) UQ and (b) MQ sites optimized by QM/MM method. The red, blue, and black lines represent the anion, neutral, and X-ray(2PRC)[57] structures, respectively.

TABLE 5: Summary of the Calculated Reaction Energy for the Electron Transfers[a]

	$H_L \rightarrow MQ$	$MQ \rightarrow UQ$
C+Res+RF+ES(P^+)[b]	−12.1	−1.5
C+Res+SCRF+ES(P^+)[b]	−6.9	−5.1
Exptl.	−15.0[c]	−1.75[d]

[a] The QM/MM optimized geometries are used. [b] See footnotes in Table 3. [c] Reference 47. [d] Reference 48.

TABLE 6: Solvation Effect of Ubiquinone Calculated by the Self-Consistent Reaction Field with the SCIPCM

method	neutral	anion	vertical EA
6-31g(d) basis sets			
gas phase	−689.129481	−689.166174	23.0
with SCRF	−689.135636	−689.219399	52.6
solv. effect (kcal/mol)	−3.9	−33.4	
6-31+g(d) basis sets			
gas phase	−689.154901	−689.209194	34.1
with SCRF	−689.161334	−689.257085	60.1
solv. effect (kcal/mol)	−4.0	−30.1	
Δ(solv. effect)[b] (kcal/mol)	−0.1	3.3	
6-31+g(d) + (SCRF)[c]	−689.161056	−689.262419	63.6

[a] X-ray geometry was used. [b] Difference in the solvation effect calculated by the 6-31g(d) and 6-31+g(d) basis sets. [c] Solvation effect calculated with the 6-31g(d) basis sets is added to the 6-31+g(d) results in the gas phase.

gave results comparable to the experimental findings, which are summarized in Table 5.

The computed reaction energy can be decomposed into the vertical electron affinity term and the relaxation energy term in a DFA. The results of this analysis clearly show that the most important term is the *vertical electron affinity of the chromophores in the protein environment*, indicating that the protein, *especially the local environment*, plays a decisive role that determines the energetics of the electron transfer. The effects of the rest of the protein, namely, the distant residues, should be less important based on our results, because our cluster models give the primarty contribution to the energetics. For the structural relaxation effect, a comparison of the results obtained with the gas-phase model and the QM/MM model indicates that there may be protein strain that restricts structural relaxation of the chromophores.

From the optimized structures, the reaction coordinate of the electron transfers can be deduced. The QM/MM optimized structures obtained for the anion and neutral states show that specific and significant reorganization of the protein structure and the solvation structure were not seen in the area of the binding site. Only slight structural relaxation caused by the electron transfers is found in the binding-site protein residues, the positions of the chromophores in their binding sites, and the skeleton structures of the chromophores.

Acknowledgment. The computations were performed using the NEC SX-5 computer at the Research Center for Computational Science, Okazaki National Research Institute. This study was supported by a Grant-in-Aid for Creative Scientific Research from the Ministry of Education, Culture, Sports, Science and Technology (MEXT) of Japan, the Matsuo Foundation, the Japanese Society for the Promotion of Science, and the U.S. National Institutes of Health.

Appendix

In some of the SCRF calculations for the binding-site models, the SCF calculations did not converge when diffuse basis sets were included. Therefore, we estimated the SCRF effect for 6-31+g(d) basis sets by that without diffuse functions as follows:

$$E(\text{6-31+g(d), SCRF}) = E(\text{6-31+g(d), vacuum}) + \{E(\text{6-31g(d), SCRF}) - E(\text{6-31g(d), vacuum})\}$$

This means that the additivity of the SCRF effect is assumed as in the ONIOM method.[77,78] This was checked for UQ as shown in Table 6. The vEA with 6-31+g(d) was 60.1 kcal/mol, whereas the estimated vEA was 63.6 kcal/mol. The Error was 3.5 kcal/mol in this scheme.

References and Notes

(1) Voet, D.; Voet, J. G. *Biochemistry*, 2nd ed.; John Wiley & Sons: New York, 1995; Chapter 22.
(2) Feher, G.; Allen, J. P.; Okamura, M. Y.; Rees, D. C. *Nature* **1989**, *339*, 111−116.
(3) Gunner, M. R. *Curr. Top. Bioenerg.* **1991**, *16*, 319−367.
(4) Deisenhofer, J.; Norris, J. R. *The Photosynthetic Reaction Center*; Academic Press: San Diego, CA, 1993; Vols. 1 and 2.
(5) Michel-Beyerle, M.-E., Ed.; *The Reaction Center of Photosynthetic Bacteria*; Springer-Verlag: Berlin, 1996.
(6) Deisenhofer, J.; Epp, O.; Miki, K.; Huber, R.; Michel, H. *J. Mol. Biol.* **1984**, *180*, 395.
(7) Abola, E. E.; Bernstein, F. C.; Bryant, S. H.; Koetzle, T. F.; Weng, J. *Protein Data Bank*, In *Crystallographic Databases—Information Content, Software Systems, Scientific Applications*; Allen, F. H., Bergerhoff, G., Sievers, R., Eds.; Data Commission of the International Union of Crystallography: Cambridge, U.K., 1987; pp. 107−132. Bernstein, F. C.; Koetzle, T. F.; Williams, G. J. B.; Meyer, E. F., Jr.; Brice, M. D.; Rodgers, J. R.; Kennard, O.; Shimanouchi, T.; Tasumi, M. The Protein Data Bank: a Computer-based Archival File for Macromolecular Structures. *J. Mol. Biol.* **1977**, *112*, 535.
(8) Warshel, A.; Parson, W. W. *J. Am. Chem. Soc.* **1987**, *109*, 6143−6152.
(9) Parson, W. W.; Warshel, A. *J. Am. Chem. Soc.* **1987**, *109*, 6152−6163.

(10) Scherer, O. J.; Scharnagl, C.; Fischer, S. F. *Chem. Phys.* **1995**, *197*, 333.
(11) Thompson, M. A.; Zerner, M. C. *J. Am. Chem. Soc.* **1992**, *113*, 8210.
(12) Nakatsuji, H.; Hasegawa, J.; Ohkawa, K. *Chem. Phys. Lett.* **1998**, *296*, 499.
(13) Hasegawa, J.; Ohkawa, K.; Nakatsuji, H. *J. Phys. Chem. B* **1998**, *102*, 10410.
(14) Plato, M.; Möbius, K.; Michel-Beyerle, M. E.; Bixon, M.; Jortner, J. *J. Am. Chem. Soc.* **1988**, *110*, 7279.
(15) Michel-Beyerle, M. E.; Plato, M.; Deisenhofer, J.; Michel, H.; Bixon, M.; Jortner, J. *Biochim. Biophys. Acta* **1988**, *932*, 52.
(16) Gunner, M. R.; Nicholls, A.; Honig, B. *J. Phys. Chem.* **1996**, *100*, 4277.
(17) Kitao, O.; Aoki, K.; Ogawa, T. *Nonlinear Opt.* **2000**, *26*, 1; **2000**, *26*, 265; *J. Computer-Aided Chem.* **2000**, *1*, 57.
(18) Marchi, M.; Gehlen, J. N.; Chandler, D.; Newton, M. D. *J. Am. Chem. Soc.* **1993**, *115*, 4178.
(19) Marcus, R. A.; Sutin, N. *Biochim. Biophys. Acta* **1985**, *811*, 265−322.
(20) Nakatsuji, H. *Chem. Phys. Lett.* **1978**, *59*, 362; **1979**, *67*, 329; **1979**, *67*, 334. Nakatsuji, H. In *Computational Chemistry, Reviews of Current Trends*; Leszezynski, J., Ed.; World Scientific: Singapore, 1996; Vol. 2, pp 62−124.
(21) Hasegawa, J.; Nakatsuji, H. *J. Phys. Chem. B* **1998**, *102*, 10420−10430.
(22) Okamura, M. Y.; Paddock, M. L.; Graige, M. S.; Feher, G. G. *Biochim. Biophys. Acta* **2000**, *1458*, 148−163.
(23) Kirmaier, C.; Holten, D.; Parson, W. W. *Biochim. Biophys. Acta* **1985**, *810*, 33−48.
(24) Stowell, M. H. B.; McPhillips, T. M.; Rees, D. C.; Soltis, S. M.; Abresch, E. *Science* **1997**, *276*, 812−816.
(25) Graigh, M. S.; Feher, G.; Okamura, M. Y. *Proc. Natl. Acad. Sci. U.S.A.* **1998**, *95*, 11679−11684
(26) Warshel, A.; Chu, Z. T.; Parson, W. W. *Science* **1989**, *246*, 112.
(27) Nonella, M.; Schulten, K. *J. Phys. Chem.* **1991**, *95*, 2059.
(28) Xu, D.; Schulten, K. *Chem. Phys.* **1994**, *182*, 91. Schulten, K.; Tesch, M. *Chem. Phys.* **1991**, *158*, 421.
(29) Rabenstein, B.; Ullmann, G.; Knapp, E.-W. *Biochemistry* **1998**, *37*, 2488−2495.
(30) Rabenstein, B.; Ullmann, G.; Knapp, E.-W. *Biochemistry* **2000**, *39*, 10487−10496.
(31) Lancaster, C. R. D.; Michel, H.; Honig, B.; Gunner, M. R. *Biophys. J.* **1996**, *70*, 2469−2492
(32) Alexov, E. G.; Gunner, M. R. *Biochemistry*, **1999**, *38*, 8253−8270.
(33) Alexov, E.; Miksovska, J.; Baciou, L.; Schiffer, M.; Hanson, D. K.; Sebban, P.; Gunner, M. R. *Biochemistry*, **2000**, *39*, 5940−5952.
(34) Datta, S. N.; Mallik, B. *Int. J. Quantum Chem.* **1997**, *61*, 865−879.
(35) Donato, M. D.; Borrelli, R.; Capobianco, A.; Monaco, G.; Improta, R.; Brahimi, M.; Peluso, A. *Adv. Quantum Chem.* **1999**, *36*, 301−322.
(36) Blomberg, M. R. A.; Siegbahn, P. E. M.; Babcock, G. T. *J. Am. Chem. Soc.* **1998**, *120*, 8812−8824.
(37) Miertus, S.; Scrocco, E.; Tomasi, J. *Chem. Phys.* **1981**, *55*, 117. Tomasi, J.; Bonnacorsi, R.; Cammi, R.; Valle, F. O. J. *J. Mol. Struct.* **1991**, *234*, 401. Tomasi, J.; Persico, M. *Chem. Rev.* **1994**, *94*, 2027.
(38) Wiberg, K. B.; Rablen, P. R.; Rush, D. J.; Keith, T. A. *J. Am. Chem. Soc.* **1995**, *117*, 4261. Wiberg, K. B.; Keith, T. A.; Frisch, M. J.; Murcko, M. *J. Phys. Chem.* **1995**, *99*, 9072.
(39) Itoh, H.; Nakatsuji, H. *J. Comput. Chem.* **2001**, *22*, 265−272.
(40) Davis, M. S.; Forman, A.; Hanson, L. L.; Fajer, J. *J. Phys. Chem.* **1974**, *83*, 3325.
(41) Wraight, C. In *Photosynthesis*: *Mechanisms and Effects*; Garab, G., Ed.; Kluwer Academic Publishers: Dordrecht, The Netherlands, 1998; pp 693−698.
(42) Heinis, T.; Chowdhury, S.; Scott, S. L.; Kebarle, P. *J. Am. Chem. Soc.* **1988**, *110*, 400−407.
(43) Schiedt, J.; Weinkauf, R. *J. Chem. Phys.* **1999**, *110* 304.
(44) Zhang, Y.; Liu, H.; Yang, W. *J. Chem. Phys.* **1999**, *110*, 46−54.
(45) Liu, H.; Zhang, Y.; Yang, W. *J. Am. Chem. Soc.* **2000**, *122*, 6560−6570.
(46) Zhang, Y.; Liu, H.; Yang, W. *J. Chem. Phys.* **2000**, *112*, 3483−3492.
(47) Woodbury, N. W. T.; Parson, W. W. *Biochim. Biophys. Acta* **1987**, *767*, 345−361.
(48) Baciou, L.; Sinning, I.; Sebban, P. *Biochemistry* **1991**, *30*, 9110−9116.
(49) Ohkawa, K.; Hada, M.; Nakatsuji, H. *J. Porphyrins Phthalocyanines* **2001**, *5*, 256.
(50) Ohtsuka, Y.; Ohkawa, K.; Nakatsuji, H.; *J. Comput. Chem.* **2001**, *22*, 521.
(51) Onsanger, L. *J. Am. Chem. Soc.* **1936**, *58*, 1486.
(52) Elstner, M.; Porezag, D.; Jungnickel, G.; Elstner, J.; Haugk, M.; Frauenheim, T.; Suhai, S.; Seifert, G. *Phys. Rev.* **1998**, *B28*, 7260−7268.
(53) Frauenheim, Th.; Seifer, G.; Elstner, M.; Hajnal, Z.; Jungnickel, G.; Porezag, D.; Suhai, S.; Scholz, R. *Phys. Status Solid.* **2000**, *217*(b), 41.
(54) Liu, H.; Elstner, M.; Kaxiras, E.; Frauenheim, T.; Hermans, J.; Yang, W. *PROTEINS*: *Struct., Funct., Genet.* **2001**, *44*, 484−489.
(55) Ponder, J. W. *TINKER, Software Tools for Molecular Design*, Version 3.6 (The most updated version for the TINKER program can be obtained from J. W. Ponder's World Wide Web site at http://dasher.wustl.edu/tinker., February 1998).
(56) Cornell, W. D.; Cieplak, P.; Bayly, C. I.; Gould, I. R.; Merz, K. M., Jr.; Ferguson, D. M.; Spellmeyer, D. C.; Fox, T.; Caldwell, J. W.; Kollman, P. A. *J. Am. Chem. Soc.* **1995**, *117*, 5179−5197 (Current parameter values are available from the AMBER site at Peter Kollman's lab at UCSF, http://www.amber.ucsf.edu/amber/amber.html).
(57) Lancaster, C. R.; Michel, H. *Structure* **1997**, *5*, 1339.
(58) Hohenberg, P.; Kohn, W. *Phys. Rev.* **1964**, *136*, B864.
(59) Kohn, W.; Sham, L. J. *Phys. Rev.* **1965**, A1133.
(60) Salahub, D. R.; Zerner, M. C., Eds.; *The Challenge of d and f Electrons*, ACS: Washington, DC, 1989.
(61) Parr, R. G.; Yang, W. *Density-functional Theory of Atoms and Molecules*; Oxford University Press: Oxford, U.K., 1989.
(62) Lee, C.; Yang, W.; Parr, R. G. *Phys. Rev. B.* **1988**, *37*, 785.
(63) Becke, A. D. *J. Chem. Phys.* **1993**, *98*, 5648.
(64) Hehre, W. J.; Ditchfield, R.; Pople, J. A. *J. Chem. Phys.* **1972**, *56*, 2257.
(65) Hariharan, P. C.; Pople, J. A. *Theor. Chim. Acta* **1973**, *28*, 213.
(66) Clark, T.; Chandrasekhar, J.; Schleyer, P. V. R. *J. Comput. Chem.* **1983**, *4*, 294.
(67) Krishnan, R.; Binkley, J. S.; Seeger, R.; Pople, J. A. *J. Chem. Phys.* **1980**, *72*, 650.
(68) Frisch, M. J.; Pople, J. A.; Binkley, J. S. *J. Chem. Phys.* **1984**, *80*, 3265.
(69) Further augmentation of the basis sets from 6-31+G(d) still causes energy lowering, as seen in Table 1. We note that the total energy is not invariant with the 6-31+G(d) set, but the effects of additional basis sets cancel each other between neutral and anion species.
(70) Pou-Amérigo, R.; Serrano-Andrés, L.; Merchán, M.; Ortí, E.; Forshberg, N. *J. Am. Chem. Soc.* **2000**, *122*, 6067−6077.
(71) Honda, Y.; Hada, M.; Nakatsuji, H. *J. Phys. Chem. A* **2002**, *106*, 3838−3849.
(72) Frisch, M. J.; Trucks, G. W.; Schlegel, H. B.; Scuseria, G. E.; Robb, M. A.; Cheeseman, J. R.; Zakrzewski, V. G.; Montgomery, J. A., Jr.; Stratmann, R. E.; Burant, J. C.; Dapprich, S.; Millam, J. M.; Daniels, A. D.; Kudin, K. N.; Strain, M. C.; Farkas, O.; Tomasi, J.; Barone, V.; Cossi, M.; Cammi, R.; Mennucci, B.; Pomelli, C.; Adamo, C.; Clifford, S.; Ochterski, J.; Petersson, G. A.; Ayala, P. Y.; Cui, Q.; Morokuma, K.; Malick, D. K.; Rabuck, A. D.; Raghavachari, K.; Foresman, J. B.; Cioslowski, J.; Ortiz, J. V.; Stefanov, B. B.; Liu, G.; Liashenko, A.; Piskorz, P.; Komaromi, I.; Gomperts, R.; Martin, R. L.; Fox, D. J.; Keith, T.; Al-Laham, M. A.; Peng, C. Y.; Nanayakkara, A.; Gonzalez, C.; Challacombe, M.; Gill, P. M. W.; Johnson, B. G.; Chen, W.; Wong, M. W.; Andres, J. L.; Head-Gordon, M.; Replogle, E. S.; Pople, J. A. *Gaussian 98*, revision A.8; Gaussian, Inc.: Pittsburgh, PA, 1998.
(73) Frisch, M. J.; Trucks, G. W.; Schlegel, H. B.; Gill, P. M. W.; Johnson, B. G.; Robb, M. A.; Cheeseman, J. R.; Keith, T.; Petersson, G. A.; Montgomery, J. A.; Raghavachari, K.; Al-Laham, M. A.; Zakrzewski, V. G.; Ortiz, J. V.; Foresman, J. B.; Cioslowski, J.; Stefanov, B. B.; Nanayakkara, A.; Challacombe, M.; Peng, C. Y.; Ayala, P. Y.; Chen, W.; Wong, M. W.; Andres, J. L.; Replogle, E. S.; Gomperts, R.; Martin, R. L.; Fox, D. J.; Binkley, J. S.; Defrees, D. J.; Baker, J.; Stewart, J. P.; Head-Gordon, M.; Gonzalez, C.; Pople, J. A. *Gaussian 94*, revision E.2; Gaussian, Inc.: Pittsburgh, PA, 1995.
(74) Nagel, J. F.; Tristram-Nagle, S. *J. Membr. Biol.* **1983**, *74*, 1.
(75) Takahashi, E.; Wraight, C. A. *Biochim. Biophys. Acta* **1990**, *1020*, 107.
(76) Paddock, M. L.; Rongey, S. H.; McPherson, P. H.; Feher, G.; Okamura, M. Y. *Biophys. J.* **1991**, *59*, 142a.
(77) Maseras, F.; Morokuma, K. *J. Comput. Chem.* **1995**, *16*, 1170.
(78) Svensson, M.; Humbel, S.; Froese, R. D. J.; Matsubara, T.; Sieber, S.; Morokuma, K. *J. Phys. Chem.* **1996**, *100*, 19357.